Noninvasive in vivo optical detection of biofilm in the human middle ear

Cac T. Nguyen[a,b], Woonggyu Jung[a], Jeehyun Kim[c], Eric J. Chaney[a], Michael Novak[d], Charles N. Stewart[e,f], and Stephen A. Boppart[a,b,g,h,1]

[a]Beckman Institute for Advanced Science and Technology and [b]Department of Electrical and Computer Engineering, University of Illinois at Urbana–Champaign, Urbana, IL 61801; [c]Department of Electrical and Computer Engineering, Kyungpook National University, Daegu 702-701, Korea; [d]Department of Otolaryngology, Carle Foundation Hospital, Urbana, IL 61801; [e]Blue Highway, LLC, Syracuse, NY 13244; [f]Welch Allyn, Inc., Skaneateles Falls, NY 13153; and [g]Department of Bioengineering and [h]Department of Internal Medicine, University of Illinois at Urbana–Champaign, Urbana, IL 61801

Edited by E. Peter Greenberg, University of Washington, Seattle, WA, and approved April 23, 2012 (received for review January 27, 2012)

Otitis media (OM), a middle-ear infection, is the most common childhood illness treated by pediatricians. If inadequately treated, OM can result in long-term chronic problems persisting into adulthood. Children with chronic OM or recurrent OM often have conductive hearing loss and communication difficulties and require surgical treatment. Tympanostomy tube insertion, the placement of a small drainage tube in the tympanic membrane (TM), is the most common surgical procedure performed in children under general anesthesia. Recent clinical studies have shown evidence of a direct correspondence between chronic OM and the presence of a bacterial biofilm within the middle ear. Biofilms are typically very thin and cannot be recognized using a regular otoscope. Here we report the use of optical coherent ranging techniques to noninvasively assess the middle ear to detect and quantify biofilm microstructure. This study involves adults with chronic OM, which is generally accepted as a biofilm-related disease. Based on more than 18,537 optical ranging scans and 742 images from 13 clinically infected patients and 7 normal controls using clinical findings as the gold standard, all middle ears with chronic OM showed evidence of biofilms, and all normal ears did not. Information on the presence of a biofilm, along with its structure and response to antibiotic treatment, will not only provide a better fundamental understanding of biofilm formation, growth, and eradication in the middle ear, but also may provide much-needed quantifiable data to enable early detection and quantitative longitudinal treatment monitoring of middle-ear biofilms responsible for chronic OM.

optical coherence tomography | primary care imaging | low-coherence interferometry | otoscopy | otolaryngology

Otitis media (OM) is a middle-ear infection often caused by bacteria growth between the tympanic membrane (TM) and the inner ear. Middle-ear infections occur in approximately 75% of children by age 3 y, and ear infections are the most common childhood illness treated by pediatricians (1, 2). Young children often acquire ear infections after upper respiratory tract infections or allergic reactions to foods or environmental allergens. Adults account for almost 20% of the annual visits for OM (3). Characterization of middle-ear infections is currently based on symptoms, duration, otoscopic observation, and physical diagnosis. The most common type is acute OM (AOM), a rapid-onset infection with one or more symptoms including otalgia, fever, and irritability. In AOM, physicians often see an abnormal-appearing TM on pneumatic otoscopy, including bulging, opacity, effusion, and decreased mobility. Most cases of AOM clear in 1 or 2 w, and antibiotics are frequently used. Recurrent AOM and OM with effusion are considered chronic OM. These diseases often cause long-term or permanent ear damage, which is linked to hearing loss and speech delay in small children if inadequately treated. Most cases of chronic OM do not respond to antibiotic treatment (4, 5), and thus surgery to place a tympanostomy tube in the TM is often recommended for continuous ventilation (6). This surgery is the second most common surgical procedure performed in young children (after circumcision) and is the most common surgical procedure in young children performed under general anesthesia. Debate is ongoing regarding the appropriate use of antibiotics in all types of OM, indicating a strong need for additional quantitative data or biomarkers to help determine optimal treatment strategies and more effectively manage these common diseases.

The diagnosis of chronic OM is one of the most challenging in the management of middle-ear infection. Unlike in AOM, most patients with chronic OM do not have noticeable symptoms, and the physical evidence of chronic OM is challenging to detect by current clinical methods. Standard otoscopy is used most frequently in the diagnosis of chronic OM; however, the accuracy of this method is limited, with a sensitivity of 74% and specificity of 60% (7, 8). Other currently available diagnostic methods, including pneumatic otoscopy and tympanometry, can yield slightly higher sensitivities and specificities (70–90%) than standard otoscopy under ideal conditions (7, 8). In both pneumatic otoscopy and tympanometry, technical problems can interfere with obtaining a good seal within the patient's ear canal, affecting the accuracy and reliability of measurements. Accurate measurements require use of a proper-sized ear speculum and depend heavily on physician expertise and patient cooperation. The accuracy of these measurements also can be affected by other factors, including cerumen and instrument pressure. Therefore, a combination of the three methods—otoscopy, pneumatic otoscopy, and tympanometry, if necessary, is now recommended for the diagnosis of chronic OM (7, 8). Although these methods are helpful in detecting effusions in chronic OM, they have a limited ability to qualitatively or quantitatively track changes in effusions during treatment.

Recent clinical studies have shown that chronic OM is strongly associated with the presence of a bacterial biofilm behind the TM (9). A biofilm is a complex self-assembled habitat of multiple species of microorganisms (e.g., bacteria, fungi, viruses) that grow communally in an adhesive biopolymer matrix. Middle-ear mucosal specimens from 26 patients with OM with effusion or recurrent OM were surgically removed, cultured, and visualized by confocal laser scanning microscopy, and 92% of these specimens showed bacterial biofilms (9). Biofilms were not observed in mucosal specimens from uninfected ears from control patients undergoing placement of cochlear implants (9). Studies have also observed biofilm formation in induced chronic OM in animal models. The pathogenic bacteria *Pseudomonas aeruginosa*, which exists in virtually all infected middle-ear cultures, was shown to form a biofilm in the middle ear of a nonhuman primate model (10). The relationship between chronic OM and bacterial biofilms has also been supported in various pathology studies, with the presence of a biofilm identified as the common cause of persistent infections. The microstructure of biofilms was found to be highly

Author contributions: C.T.N. and S.A.B. designed research; C.T.N., E.J.C., and M.N. performed research; C.T.N., W.J., J.K., and C.N.S. contributed new reagents/analytic tools; C.T.N. and S.A.B. analyzed data; and C.T.N. and S.A.B. wrote the paper.

The authors declare no conflict of interest.

This article is a PNAS Direct Submission.

[1]To whom correspondence should be addressed. E-mail: boppart@illinois.edu.

This article contains supporting information online at www.pnas.org/lookup/suppl/doi:10.1073/pnas.1201592109/-/DCSupplemental.

heterogeneous in composition and architecture, including cell distribution, cell aggregation, structural voids, and fluid channels. Within biofilms, microbes are protected from harsh environments, including exposure to antibiotic or biocide treatments, supporting a cycle of increasing antibiotic resistance and reseeding of recurrent or persistent infections (11–13).

Whereas standard otoscopy relies on illumination and magnification of the TM surface, it is not effective for visualizing structures within the middle ear, especially when the TM is no longer translucent in states of disease. Low-coherence interferometry (LCI) and optical coherence tomography (OCT) refer to the same basic optical ranging technique that uses an interferometer and low-coherence light. In an LCI/OCT setup, a broadband optical light source is used to generate low-coherence light, which is then split by a beam splitter or fiberoptic coupler and sent to a sample arm and a reference arm of the interferometer. The reference arm contains a stationary mirror, and the sample arm contains beam-delivery optics to direct the beam toward the sample. The fiber-optics and micro-optics within the sample arm are also highly amenable to integration with a standard or video otoscope. The interference of the two back-reflected or scattered beams is captured by a linear photodetector array and processed by a computer to describe the depth-resolved optical scattering properties of the tissue. In an OCT system, adjacent LCI-acquired depth scans are assembled to generate a cross-sectional image of tissue, as the beam is transversely (laterally) scanned. The broadband, near-infrared light used in LCI/OCT allows for axial resolutions of up to 2–3 μm and penetration depths of up to 2–3 mm in highly scattering tissues, depending on tissue type. The spatial variations in the optical backscattered signal are displayed as images and used to describe the tissue microstructures (14, 15).

The noninvasive, high-resolution depth-ranging and imaging capabilities of LCI/OCT offer the potential for applications in the middle ear, specifically for the detection and quantification of middle-ear biofilms (16, 17). With micrometer-scale resolution, OCT is capable of imaging the microstructure of biofilms, including the dynamics of biofilm formation, as demonstrated in a laboratory flow-cell experiment in which the 3D structure was visualized over time (18). Three-dimensional OCT imaging has been performed on ex vivo human ear structures to reveal the microstructures of the middle ear, including the TM, malleus, incus, chorda tympani nerve, and tendon of the tensor tympani muscle (16). LCI data alone have been used to efficiently classifying human breast tissue types (19), suggesting that a similar application is possible to quantitatively characterize middle-ear structures and classify OM status.

In our previous research to motivate and support this human study, we demonstrated the utility of LCI/OCT for investigating the presence of bacterial biofilms in the middle ear (20) using a rat model developed to induce and grow biofilms (21). The additional scattering layers observed behind the TM using LCI/OCT were histologically confirmed to be biofilms. The TM and any accompanying biofilm appear in LCI/OCT data as distinct scattering signals and layers. The layers from each axial scan were analyzed in terms of three different parameters: thickness of TM with or without a biofilm layer, intensity of optical backscatter, and optical attenuation through the structures. The statistical results of axial scan classification can be used to determine the likelihood of a biofilm being present, and can provide a quantitative parameter for diagnosing OM and monitoring treatment.

Studies have established a clear and direct link between chronic OM and middle-ear biofilms in humans based on invasive mucosal sampling followed by microscopy (9), and LCI/OCT imaging of middle-ear biofilms has been demonstrated in an animal model (20, 21). In this work, we demonstrate the application of middle-ear imaging by in vivo LCI/OCT in adult patients for the detection and classification of biofilms. We used both an LCI-otoscope system and a 2D cross-sectional imaging OCT otoscope system to generate LCI depth scans, which we classified and used to identify the presence of biofilms in the middle ear of 20 human subjects. The visualization of normal TMs without biofilms and TMs with representative biofilms of different structures demonstrates the capability of LCI/OCT for middle-ear diagnostics and imaging, and suggests their further use in diagnosing middle-ear biofilms and monitoring biofilm dynamics during the treatment of OM.

Results

Representative LCI and OCT data from a cohort of patients and normal controls (Table 1) are presented in Figs. 1–3. Approximately 18,537 LCI scans and 742 OCT images were acquired from each subject, depending on which system was used and the duration of the imaging session. Each OCT image also provided LCI data for classification and analysis, given that each OCT image comprised 1,000 adjacent but spatially separated LCI scans.

In the normal human ear, the TM appears translucent to opaque under video otoscopy (Fig. 1*A*). In a typical LCI scan for a normal ear (Fig. 1*B*), the TM is readily identified by two sharp peaks ~95 μm apart, consistent with the average thickness of the

Table 1. Summary of clinical LCI/OCT study subjects

Subject	LCI data (*n*, A%)	Clinical record	Subject	LCI data (*n*, A%)	OCT data (*n*, A%)	Clinical record
V1	N (807, 2%)	Normal	Pt8	NA	N (1500, 1%)	Normal
V2	N (430, 0%)	Normal	Pt9	NA	P (1500, 54%)	Effusion
V3	N (514, 1%)	Normal	Pt10	NA	N (1500, 11%)	Normal, debris across the TM
V4	N (434, 4%)	Normal	Pt11	N (342, 0%)	N (1500, 0%)	Tube, thin TM
Pt1	P (132, 57%)	TM retracted with fluid	Pt12	P (256, 62%)	P (1500, 71%)	Tube, healed drum
Pt2	P (218, 70%)	Persistent fluid for several years	Pt13	P (182, 76%)	P (1500, 73%)	Infected, injected drum
Pt3	P (182, 73%)	Thick TM, fluid	Pt14	P (247, 88%)	P (1500, 95%)	Dull and thick TM, tube, no active infection
Pt4	P (146, 90%)	Tube placed and removed	Pt15	NA	P (1500, 58%)	Fluid
Pt5	P (245, 63%)	Persistent fluid 6 mo after tube placed	Pt16	P (332, 57%)	P (1500, 63%)	Fluid
Pt6	P (303, 87%)	Persistent effusion				
Pt7	P (267, 37%)	History of effusion, tube replaced				

NA, not available. Data were collected from 20 TMs from 20 human subjects, including 16 patients (Pt) with a clinical history of middle-ear infection and 4 healthy volunteer controls (V). Under the LCI and OCT data columns, a classified diagnosis is listed as either negative (N) or positive (P) for a biofilm based on the total number of LCI scans (*n*) and the percent classified as abnormal (A%). Notes from the clinical record based on physician otoscopic examination observations are also listed.

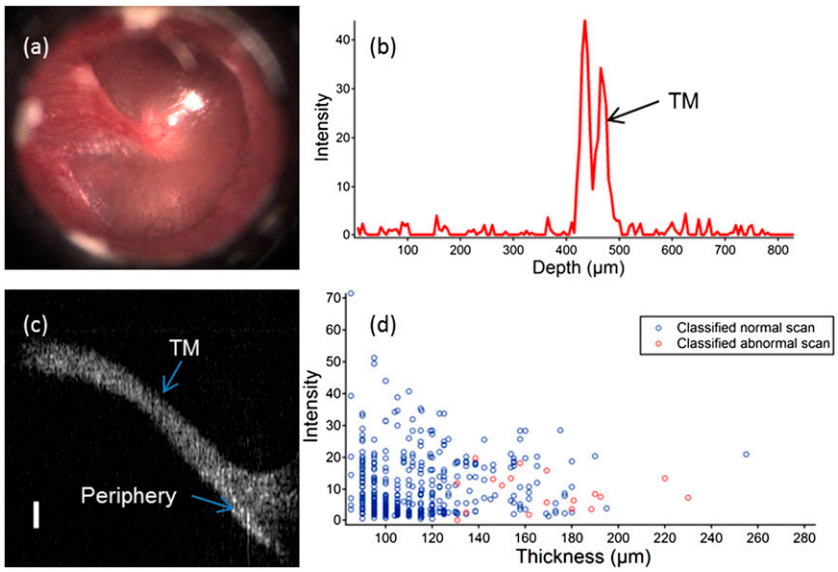

Fig. 1. Normal ear. (*A*) Video otoscope image of the TM from a normal human ear. (*B* and *C*) Typical LCI depth scan (*B*) and cross-sectional OCT image (*C*) of the TM. Based on the scattering properties of the TM, a thickness of ~95 μm was measured, which was consistent with the average thickness (100 μm) of the adult human TM. (*D*) Classification of the LCI scans from this normal ear, resulting in 98% normal scans and 2% abnormal scans. The circles represent LCI scans from a normal ear in terms of thickness and intensity. Blue and red circles represent the scans classified as normal and abnormal, respectively. (Scale bar in *C*: 100 μm.)

human TM (100 μm) (22). The classification of LCI scans from this normal ear resulted in 98% (n = 789) normal scans and 2% (n = 18) abnormal scans. The abnormal scans were likely misclassified because they were acquired from peripheral locations or the site of attachment of the malleus to the TM. The OCT image of this normal TM (Fig. 1*C*) shows a region of significantly increased membrane thickness near the periphery compared with the center.

The majority of the patients in our cohort with chronic OM presented to their physician with symptoms of hearing loss and had a middle-ear effusion detected on standard otoscopy or tympanometry. Under video otoscopy, the TM appeared red, cloudy, or retracted. These patients were assessed with LCI/OCT, and many cases a high percentage of LCI data was classified as abnormal, and the OCT images revealed the presence of a biofilm attached to a major portion of the TM. In these ears, the biofilms were typically thick and highly scattering. As a representative example, data from a patient with chronic OM and a thick, highly scattering biofilm (patient 6) are shown in Fig. 2. The video otoscopy image of this TM appears cloudy (Fig. 2*A*), and the physician diagnosed OM with persistent effusion. Both LCI scans and OCT images demonstrated the presence of a thick biofilm (200 μm average) behind the TM (Fig. 2 *B* and *C*), with a large spatial extent of biofilm colonization across the TM. In the OCT images, the biofilm structure was present along the entire transverse scan. LCI signal classification for these data identified 87% (n = 303) of the scans as abnormal and 13% (n = 40) as normal (Fig. 2*D*), indicating a high probability for the presence of a large biofilm.

In other patients, more spatially localized regions of biofilm on the TM were detected by LCI/OCT. In those ears, the bacterial biofilms covered the TM only partially, in a sparse geographic pattern. The percentages of abnormal LCI scans from these ears were still significant, but the structure and scattering properties of these biofilms were less prominent. The results from a second patient (patient 16) with chronic OM and a thinner, lower-scattering biofilm are shown in Fig. 3. Based on video otoscopic examination, the patient was diagnosed with OM with effusion (Fig. 3*A*). Structure representative of a thin and lower-scattering biofilm is demonstrated in both the LCI scan data and the OCT image (Fig. 3 *B* and *C*). The classification algorithm output from the LCI scans of this ear resulted in 43% (n = 144) normal scans and 57% (n = 188) abnormal scans. In the OCT image (Fig. 3*C*),

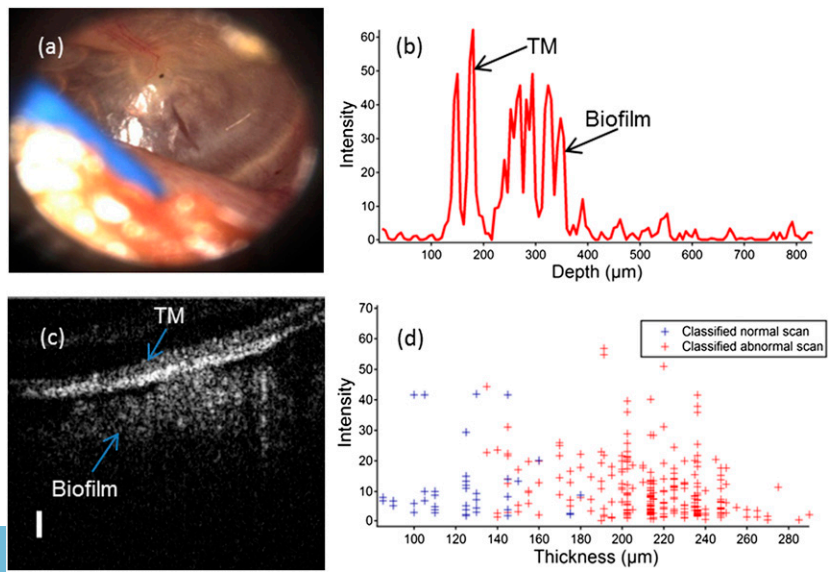

Fig. 2. Chronic middle-ear infection with a thick, highly scattering biofilm. (*A*) Video otoscopy image showing a less-translucent TM. (*B*) Typical LCI depth scan showing evidence of a thick (~200 μm average thickness) biofilm behind the TM. (*C*) Cross-sectional OCT image showing the lateral spatial extent of biofilm. (*D*) Classification results of the LCI scans demonstrating that 87% of acquired LCI scans were classified as abnormal. The crosses represent LCI scans from an abnormal ear in terms of thickness and intensity. Blue and red crosses represent the scans classified as normal and abnormal, respectively. (Scale bar in *C*: 100 μm.)

only the right portion of the TM shows obvious evidence of a biofilm. Based on all of the OCT images acquired across the TM, the sparse geographic distribution of the adherent biofilm on the TM explains the lower percentage of classified abnormal scans.

We studied 13 patients with middle-ear pathologies related to OM and 7 patients with normal ears. The LCI/OCT data collected from the seven normal ears resulted in 89–100% of the scans being classified as normal. In the first round of clinical studies (Table 1), we focused on patients with a diagnosis of chronic OM, thus increasing the probability of the presence of biofilm. Classification of LCI data from seven patients with a diagnosis of chronic OM showed a high percentage of abnormal scans in all seven, exceeding 50% in six of them. These data were strongly correlated with the clinical findings. All of these patients had fluid or an effusion present. Patient 7 was not clinically diagnosed with OM, but had an effusion detected and a tympanostomy tube placed and was being evaluated for tube dysfunction and hearing loss. This patient's 37% abnormal LCI scans suggested the persistence of residual biofilm and/or effusion after the surgery.

In the second round of experiments, both LCI and OCT systems were used to collect data from patients. Different otologic pathologies were targeted to further evaluate the performance of the classification algorithm and provide additional comparative data for physicians. To validate the classification algorithm, three typical OCT images from different locations in each patient were used to extract axial scans. These axial scans were then classified using the algorithm developed for the LCI scans. The percentage of abnormal scans out of these extracted axial scans from each patient was calculated (Table 1). Nine patients were imaged with the LCI and/or OCT systems in this round. Three patients (8, 10, and 11) had normal TMs, and 5 patients (9, 12, 13, 15, and 16) had fluid that was well correlated with the LCI/OCT data. Patient 14 clinically exhibited a dull, thick TM and was determined to be infection-free, even though the LCI/OCT data showed a large percentage of abnormal scans. The LCI/OCT data from this ear revealed an irregular biofilm/effusion structure that completely adhered to the TM, explaining the clinical observations of a thick, dull TM.

All seven of the clinically normal ears had a low percentage of abnormal LCI scans (<11%), six of which were <5%. All of the 13 patients with chronic middle-ear pathologies had abnormal LCI or OCT data, as demonstrated by the large percentage of abnormal LCI scans or abnormal LCI scans extracted from OCT images (>37%). Eleven of 12 patients (92%) with clinically diagnosed chronic OM had >50% abnormal LCI scans. Considering the relatively low percentage of abnormal LCI scans from normal ears, we set >25% abnormal LCI scans as the threshold for defining a patient with biofilm using LCI/OCT data.

Discussion and Conclusion

Quantitative characterization of AOM and chronic OM has been a critical need not only in clinical medicine, but also in medical science, to develop more fundamental insight into the etiology, dynamics, and treatment responses of middle-ear biofilms. Currently available methods for diagnosing OM, including standard otoscopy, pneumatic otoscopy, and tympanometry, have limited ability to quantify the visualized data and offer relatively low diagnostic accuracy. We report a diagnostic technique for assessing middle-ear infections using LCI and OCT that is able to noninvasively detect, quantify, and monitor middle-ear biofilms in humans.

In this clinical study, we constructed and validated LCI/OCT integrated otoscopy systems. The LCI/OCT data obtained from normal ears and from infected ears with thin, low-scattering localized biofilms or thick, higher-scattering large-area biofilms demonstrate these systems' capability and sensitivity for detecting and characterizing middle-ear biofilms. Based on our clinical study, a percentage of abnormal LCI scans exceeding 25% is considered evidence for the presence of a biofilm, whereas >70% abnormal LCI scans is considered evidence of the presence of a large biofilm occupying a significant portion of the TM. This wide range of percentage of abnormal LCI scans suggests the potential for noninvasive monitoring of spatial development and regression of biofilms within the middle ear.

The OCT images and classification results from the algorithm developed and implemented for the LCI data were in good agreement with clinical patient records and observations. Data from all 13 patients with chronic OM showed evidence of biofilms, whereas data from all 7 normal patients did not. This finding agrees with the results of a previous invasive study that directly detected the presence of biofilms in 46 of 52 patients with chronic OM using surgically removed middle-ear mucosal specimens cultured, stained, and observed by confocal laser scanning (9). It is important to note that the present study used noninvasive LCI/OCT, which is also able to longitudinally monitor changes in dynamics of middle-ear biofilms. Out of a total of 18,537 LCI scans from 20 ears, we found a sensitivity of 68% and specificity of 98% for identifying the presence of a biofilm, using clinical otoscopic observations and physical examination as the gold standard. The low sensitivity is explained by the relatively low percentage of abnormal scans in cases with evidence of a small, thin, low-scattering biofilm. Considering only the cases with evidence of a larger, thicker, more

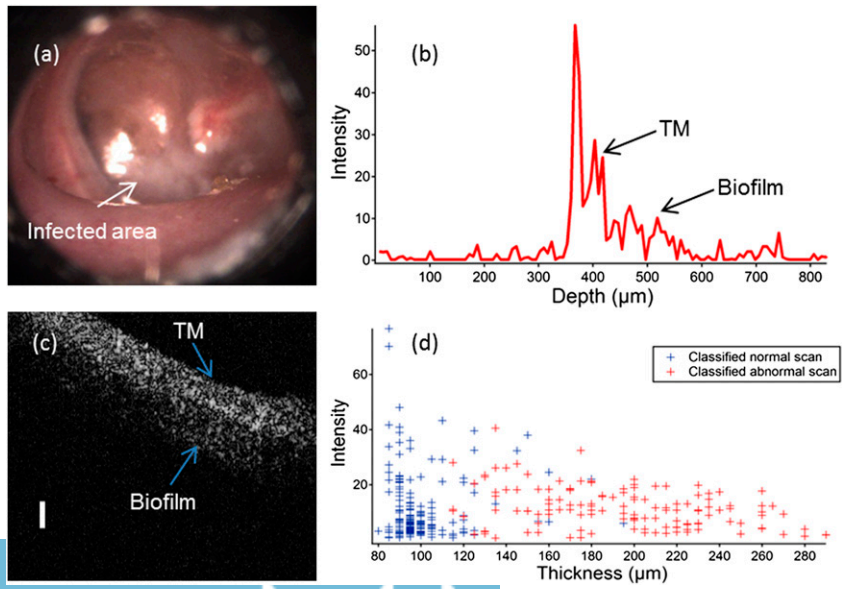

Fig. 3. Chronic middle-ear infection with thinner, lower-scattering biofilm. (*A*) Video otoscopy image showing a cloudy TM. (*B*) Typical LCI depth-scan showing evidence of a thin, low-scattering biofilm behind the TM. (*C*) Cross-sectional OCT image showing a thinner and more spatially localized biofilm. (*D*) Classification results of the LCI scans from this TM demonstrating 57% abnormal scans. Blue and red crosses represent the scans classified as normal and abnormal, respectively. The relatively low number of classified abnormal scans in this infected ear is related to the geographic pattern of developing biofilm across the TM. (Scale bar in *C*: 100 μm.)

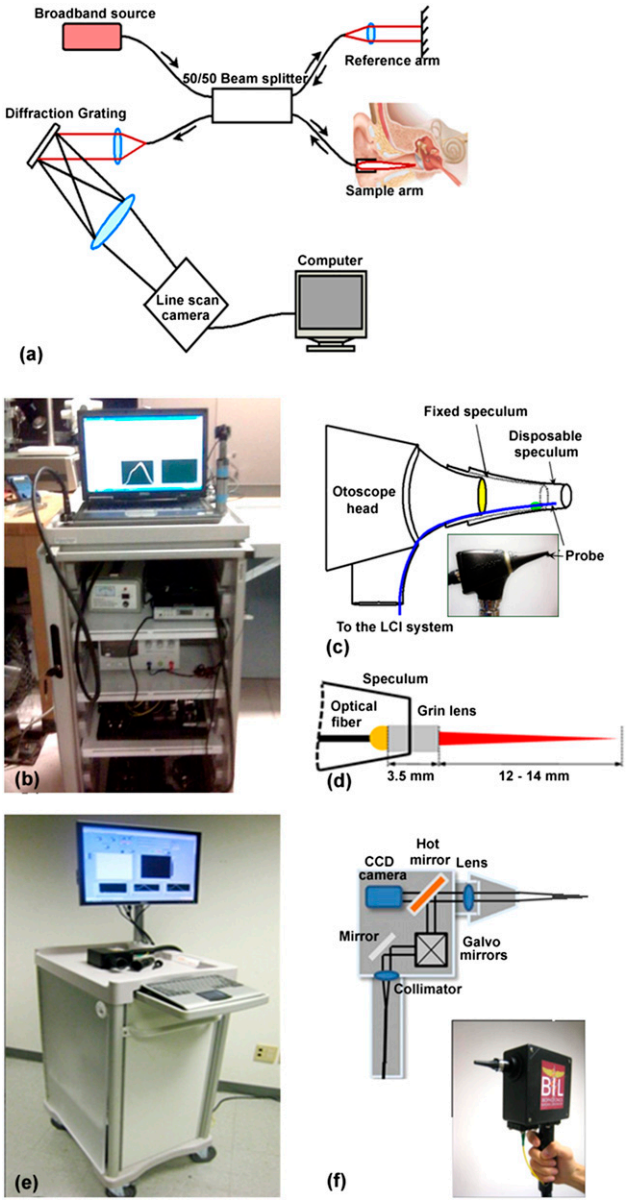

Fig. 4. Portable LCI/OCT otoscopy systems. (*A*) Schematic of the LCI/OCT optical systems. (*B*) Photograph of the portable LCI-otoscopy system. (*C*) Schematic and photograph of the integration of the LCI fiber-based micro-optic probe into the otoscope head. (*D*) Schematic and beam profile of the long-working-distance LCI probe, which uses a gradient-index (GRIN) lens. (*E*) Photograph of the portable OCT-otoscopy system. (*F*) Schematic and photograph of the OCT-otoscopy hand-held scanner. The OCT-otoscopy system enables 2D and 3D cross-sectional OCT images, in contrast to the individual LCI depth scans provided by the LCI-otoscopy system. However, the OCT-otoscopy system has added complexity because of the use of galvanometer-mounted mirrors for scanning the beam across tissue.

highly scattering biofilm, in which the percentage of abnormal scans exceeded 70%, the sensitivity was 83% and specificity was 98%. This demonstrates that LCI/OCT can readily identify normal middle ears without biofilms, and also detect highly scattering biofilms with higher accuracy than current diagnostic methods, which offer sensitivities and specificities of 70–90% (8).

In terms of technical design, both LCI and OCT demonstrate the capability to noninvasively access bacterial biofilms in the middle ear. These portable systems provide a depth resolution of ~4.5 μm and an imaging depth range of ~2 mm. Thus, LCI/OCT is capable of accessing the TM and possible biofilms, as well as any effusion in the middle ear. The LCI-otoscopy system, compared with the OCT-otoscopy system, is lower in cost and simpler in design without a transverse 2D or 3D scanning mechanism. The LCI-otoscopy system provides depth-dependent optical scattering information sampled at various locations across the TM, depending on where the beam is directed. The OCT-otoscopy system is more complex with the addition of a pair of galvanometer-mounted mirror scanners for 2D and 3D OCT imaging, but these OCT images provide a more accurate visual representation of the biofilm structure. The classification algorithm can be applied to data from either system, individual LCI scans or LCI data extracted from the OCT images. Two different center wavelengths (830 nm for OCT-otoscopy and 940 nm for LCI-otoscopy) were used in this study. Despite the slight differences in axial resolution and penetration depth, both wavelengths proved suitable for coherent optical ranging and middle-ear diagnostics.

In a previous study using a rat animal model of middle-ear biofilms (20), LCI scan locations were poorly guided by the video otoscopic images because of the narrow ear canal in this model, and OCT images of the TM were subsequently collected ex vivo. Those limitations were resolved in the present study with the larger human ear canals that allowed greater access and video image focusing, and permitted noninvasive acquisition of LCI/OCT data in vivo, guided by high-quality video otoscopy. However, in some cases, acquiring LCI/OCT data with an adequate signal-to-noise ratio was difficult because the LCI/OCT beam focus could not reach the TM through a long or tortuous ear canal. Further improvements in the LCI/OCT probe to overcome this limitation, such as an adjustable working distance and a handle with an angled head, merit study.

This initial study was limited to adult patients presenting with a wide range of medical histories of chronic OM. It will also be important to target the pediatric population of patients and differentiate between AOM and chronic OM. Because pediatric patients are often less tolerant of ear examinations, especially in the presence of an ear infection, we would expect a shorter time window for collecting LCI/OCT data. Normal TMs in children are also thinner than those in adults. Thus, the successful use of LCI/OCT in children likely will require slight modifications to the systems, including faster acquisition rates and accurate alignment of the LCI/OCT beam focus with the video otoscope focus.

Based on our initial results on detecting biofilms, it may be possible to differentiate bacterial species based on biofilm architecture and to distinguish bacterial biofilms from turbid, optically scattering effusions. Because the present study suggests the potential for using LCI/OCT to monitor biofilm growth and regression dynamics, it will be possible to track patients with repeated AOM progressing to chronic OM before and after antibiotic treatment and before and after tympanostomy tube placement. Longitudinal LCI/OCT data from a variety of clinical ear pathologies is expected to provide a useful monitoring method not only to improve patient management, but also to serve as a medical research tool to better understand the fundamental processes of biofilms and how they contribute to middle-ear diseases.

Middle-ear infections are one of the most common diseases. Detecting chronic infections, determining the need for antibiotic treatment, and tracking the response to antibiotics are the major challenges in the diagnosis and treatment of middle-ear infections. The use of LCI/OCT to noninvasively assess the middle ear for the presence of bacterial biofilm can be applied to the clinical diagnosis and management of middle-ear infections.

Materials and Methods

Instrumentation. Detection and imaging of middle-ear biofilms was performed using two systems. Compared with the OCT-otoscopy system, the LCI-otoscopy system is faster, lower cost, and more compact, with fewer requirements for mechanical beam scanning. However, each depth-resolved scan is spatially independent from the others captured during each session. The OCT-otoscopy system uses a pair of galvanometer-mounted mirrors to

scan the optical beam across tissue and assembles adjacent LCI depth scans into a 2D or 3D image. This system is more expensive to construct and more complex, but provides cross-sectional images of the TM and any biofilms, which can be more readily identified by users.

The portable LCI-otoscopy system comprises three main components: the LCI core optics, the LCI probe, and a standard video otoscope. The LCI core optics (Fig. 4*A*) uses a superluminescent diode (SLD) as the low-coherence light source for the LCI system. This SLD has a center wavelength of 940 nm and a bandwidth of 70 nm, enabling an axial resolution of ~4 μm in tissue. The interference fringes generated by back reflections from the sample and reference arms are detected by a line-scan camera (Dalsa) with 2,048 pixels, 10-μm pixel size, and 35,000-Hz line rate. The camera is connected to the laptop computer by a PCMCIA data acquisition card, which supports a Camera Link interface (Imperx) (Fig. 4*B*).

The micro-optics of the LCI probe were custom-designed with a small diameter (0.5–0.7 mm) and a long working distance (12-14 mm) to match the video otoscope optics. A gradient index (GRIN) lens with a diameter of 0.5 mm, length of ~3.5 mm, and working distance of 6 mm was initially used. The 8° polish angles of the GRIN lens prevented large back reflections from surfaces of the probe. To achieve the long working distance, this lens was then polished and glued to the fiber. The polished length of the lens and the glue layer thickness were calculated by theory and simulation in a related study (23). The final LCI probes had a long working distance in the range of 12–14 mm and a spot size of ~30 μm (transverse resolution). The distal end of this fiber probe was positioned within a plastic ear speculum tip to enable location of the focused beam within the field of view of the video otoscope image (Fig. 4 *C* and *D*). A standard video otoscope (model 23120; Welch Allyn) was used for these studies, allowing use of the real-time otoscope CCD camera video to track the location of the LCI beam incident on the TM, as well as provide digital video imaging of the TM surface illuminated with white light from the otoscope illumination source. This LCI system could readily interface with other standard (nonvideo) otoscopes as well, provided that an additional visible aiming beam was colinearly propagated with the LCI beam and incident on the TM.

The OCT-otoscopy system (Fig. 4*E*) was designed for future use in primary care imaging applications and has been described previously (24). This system was also used to compare OCT and LCI data collection, and provided image-based data at the expense of more complex and costly beam scanning hardware. In brief, this system uses an SLD light source operating at a center wavelength of 830 nm and a bandwidth of 70 nm, providing an axial resolution of ~3 μm in tissue. A high-speed line scan camera (Sprint; Basler) and frame grabber (National Instruments) enable a data acquisition rate of ~70,000 axial scans/s or an image acquisition rate of ~ 70 frames/s, with each image containing 1,000 axial scans (columns) of LCI data. Sixteen OCT images 1 × 1.5 mm in size can be displayed each second after processing. The handheld OCT scanner uses galvanometer-mounted mirrors for fast 2D and 3D image acquisition. A miniature 0.27-megapixel CCD-based color video camera (1.6 cm diameter × 2.1 cm long) is also integrated to simultaneously capture real-time video images of the TM surface during the acquisition of cross-sectional OCT images. All of the optics in the handheld scanner are packaged inside a light, robust plastic box (11.5 cm × 11.5 cm × 6.3 cm) (Fig. 4*F*). The lens mount was constructed by modifying the same metal ear tip used in existing commercial otoscopes. This allowed for the use of disposable ear specula for each patient.

Both systems were controlled by custom-written software (Labview), which included a user-friendly graphical interface to display both the CCD video image and the collected LCI data or the OCT images. Our OCT-otoscopy system also included additional features, including acquisition of orthogonal OCT images for optimal alignment and auditory indicators that informed the user of correct positioning of the handheld scanner relative to the optical focus and the tissue location. Each imaging session, including positioning the probe and acquiring LCI/OCT data, took 1–3 min, a reasonable duration for both adult and pediatric patients.

Human Subjects. A total of 20 human subjects were recruited for this study under Institutional Review Board protocols approved by both the University of Illinois at Urbana–Champaign and Carle Foundation Hospital (Table 1). Of these 20 subjects, 4 were normal volunteers and 16 were adult patients being evaluated and/or treated for chronic OM. Our LCI-otoscopy system was used on 11 subjects, and our OCT-otoscopy system was used on 9 subjects. The LCI/OCT systems were located within the outpatient examination rooms in the Otology Clinic at Carle Foundation Hospital. Data acquisition was performed for ~5–10 min immediately after the standard patient examination.

Classification Algorithm. A classification algorithm was developed to classify human middle-ear LCI scans as either normal or abnormal with biofilm or effusion present. Each LCI scan was characterized by three parameters: thickness of the TM with or without a biofilm layer, intensity of optical backscatter, and optical attenuation through the TM and any additional structures within the middle ear. Additional details on the classification algorithm are provided in *SI Materials and Methods*.

ACKNOWLEDGMENTS. We thank Dr. Peter Dragic, Department of Electrical and Computer Engineering, University of Illinois at Urbana–Champaign, for the use of fiber-splicing equipment and for technical help with the optical fibers. We also thank Barbara Hall, Katie McGlasson, Pam Leon, Meghan McCoy, and Laura Browning for their assistance in collecting clinical data at Carle Foundation Hospital. This work was supported in part by National Institutes of Health National Institute of Biomedical Engineering and Bioimaging Grant R01 EB013723 (to S.A.B.); Blue Highway, LLC; and Welch Allyn, Inc. Additional information on OCT and related optical imaging technologies can be found at http://biophotonics.illinois.edu.

1. Klein JO (1994) Otitis media. *Clin Infect Dis* 19:823–833.
2. Roberts JE, Rosenfeld RM, Zeisel SA (2004) Otitis media and speech and language: a meta-analysis of prospective studies. *Pediatrics* 113:e238–e248.
3. Culpepper L, et al. (1993) Acute otitis media in adults: a report from the International Primary Care Network. *J Am Board Family Pract* 6:333–339.
4. Froom J, et al. (1997) Antimicrobials for acute otitis media? A review from the International Primary Care Network. *BMJ* 315:98–102.
5. Hoberman A, et al. (2011) Treatment of acute otitis media in children under 2 years of age. *N Engl J Med* 364:105–115.
6. Pransky SM (1998) Surgical strategies for otitis media. *J Otolaryngol* 27(Suppl 2): 37–42.
7. Shekelle PT, et al. (2003) *Diagnosis, Natural History, and Late Effects of Otitis Media with Effusion* (Agency for Healthcare Research and Quality, Rockville, MD), Evidence Report/Technology Assessment 55.
8. Harris PK, Hutchinson KM, Moravec J (2005) The use of tympanometry and pneumatic otoscopy for predicting middle ear disease. *Am J Audiol* 14:3–13.
9. Hall-Stoodley L, et al. (2006) Direct detection of bacterial biofilms on the middle-ear mucosa of children with chronic otitis media. *JAMA* 296:202–211.
10. Dohar JE, et al. (2005) Mucosal biofilm formation on middle-ear mucosa in a non-human primate model of chronic suppurative otitis media. *Laryngoscope* 115: 1469–1472.
11. Allegrucci M, et al. (2006) Phenotypic characterization of *Streptococcus pneumoniae* biofilm development. *J Bacteriol* 188:2325–2335.
12. Potera C (1999) Forging a link between biofilms and disease. *Science* 283:1837–1839.
13. Costerton JW, Stewart PS, Greenberg EP (1999) Bacterial biofilms: A common cause of persistent infections. *Science* 284:1318–1322.
14. Drexler W, Fujimoto J (2008) *Optical Coherence Tomography: Technology and Applications* (Springer, New York).
15. Zysk AM, Nguyen FT, Oldenburg AL, Marks DL, Boppart SA (2007) Optical coherence tomography: A review of clinical development from bench to bedside. *J Biomed Opt* 12:051403.
16. Pitris C, Saunders KT, Fujimoto JG, Brezinski ME (2001) High-resolution imaging of the middle ear with optical coherence tomography: A feasibility study. *Arch Otolaryngol Head Neck Surg* 127:637–642.
17. Djalilian HR, et al. (2008) Imaging the human tympanic membrane using optical coherence tomography in vivo. *Otol Neurotol* 29:1091–1094.
18. Xi C, Marks D, Schlachter S, Luo W, Boppart SA (2006) High-resolution three-dimensional imaging of biofilm development using optical coherence tomography. *J Biomed Opt* 11:34001.
19. Zysk AM, Boppart SA (2006) Computational methods for analysis of human breast tumor tissue in optical coherence tomography images. *J Biomed Opt* 11:054015.
20. Nguyen CT, Tu H, Chaney EJ, Stewart CN, Boppart SA (2010) Non-invasive optical interferometry for the assessment of biofilm growth in the middle ear. *Biomed Opt Express* 1:1104–1116.
21. Chaney EJ, Nguyen CT, Boppart SA (2011) Novel method for non-invasive induction of a middle-ear biofilm in the rat. *Vaccine* 29:1628–1633.
22. Lim DJ (1995) Structure and function of the tympanic membrane: A review. *Acta Otorhinolaryngol Belg* 49:101–115.
23. Jung W, et al. (2010) Numerical analysis of gradient index lens-based optical coherence tomography imaging probes. *J Biomed Opt* 15:066027.
24. Jung W, et al. (2011) Handheld optical coherence tomography scanner for primary care diagnostics. *IEEE Trans Biomed Eng* 58:741–744.